From quantum pulse gate to quantum pulse shaper—engineered frequency conversion in nonlinear optical waveguides

Benjamin Brecht[1,3]**, Andreas Eckstein**[1,2]**, Andreas Christ**[1,2]**, Hubertus Suche**[1] **and Christine Silberhorn**[1,2]

[1] Applied Physics, University of Paderborn, Warbuger Strasse 100, 33098 Paderborn, Germany
[2] Max Planck Institute for the Science of Light, Günther-Scharowsky-Strasse 1/Building 24, 91058 Erlangen, Germany
E-mail: benjamin.brecht@uni-paderborn.de

Abstract. Full control over the spatiotemporal structure of quantum states of light is an important goal in quantum optics, to generate, for instance, single-mode quantum pulses or to encode information on multiple modes, enhancing channel capacities. Quantum light pulses feature an inherent, rich spectral broadband-mode structure. In recent years, exploring the use of integrated optics as well as source engineering has led to a deep understanding of the pulse-mode structure of guided quantum states of light. In addition, several groups have started to investigate the manipulation of quantum states by means of single-photon frequency conversion. In this paper, we explore new routes towards complete control of the inherent pulse-modes of ultrafast pulsed quantum states by employing specifically designed nonlinear waveguides with adapted dispersion properties. Starting from our recently proposed quantum pulse gate (QPG), we further generalize the concept of spatiospectral engineering for arbitrary $\chi^{(2)}$-based quantum processes. We analyse the sum-frequency generation-based QPG and introduce the difference-frequency generation-based quantum pulse shaper (QPS). Together, these versatile and robust integrated optical devices allow for arbitrary manipulations of the pulse-mode structure of ultrafast pulsed quantum states. The QPG can be utilized to select an

[3] Author to whom any correspondence should be addressed.

arbitrary pulse mode from a multimode input state, whereas the QPS enables the generation of specific pulse modes from an input wavepacket with a Gaussian-shaped spectrum.

Contents

1. Motivation

Ultrafast pulsed quantum states of light play an increasingly important role in quantum information and quantum communication as they allow for efficient network synchronization and high data transmission rates. In general, they feature a rich spectral mode structure, which is most naturally described on a broadband pulse-mode basis. This is not a new result in either classical or quantum optics [1]. For classical states, all basis sets are formally equivalent and no specific choice can be distinguished. In contrast, it has been shown that pulsed quantum states of light exhibit an inherent pulse-mode structure, which is solely determined by their generation process [2]. Different kinds of applications require specifically tailored pulsed quantum states, be it single-mode states for linear optical quantum computation [3] or multimode states for high-capacity quantum information encoding. Thus, a thorough understanding of the spatiospectral modal structure of ultrafast quantum states as well as the ability to exercise full control over that structure is an important goal in today's quantum optical research.

In this paper, we investigate the potential of engineered nonlinear waveguides for the manipulation of pulsed quantum states, which cannot be achieved within the framework of linear optics. Special emphasis is put on an accurate description of the $\chi^{(2)}$-process inside the guide, which takes into account rigorously the spatial and spectral degrees of freedom. Thus quantitative measures can be derived for the efficiency of practical quantum optical devices.

This paper is organized as follows. In section 2, we review the state-of-the-art methods for generating ultrafast pulsed quantum states and manipulating their inherent pulse-mode structure in bulk crystals and waveguides. We briefly discuss the latest developments and introduce new ideas by combining dispersion engineering techniques, which have become established by now for photon-pair preparation, with current methods of state manipulation utilizing $\chi^{(2)}$-nonlinearities. In this context, we analyse the experimental implementation of our recently proposed quantum pulse gates (QPG) [4] and extend the formalism further by presenting the concept of a quantum pulse shaper (QPS). In sections 3 and 4, we develop a theoretical framework for our devices. We start with the linear operator transformations for sum- and difference-frequency generation and derive the interaction Hamiltonian of these processes considering spatial and temporal degrees of freedom. Our analysis results in a completely quantitative model. Section 5 is dedicated to merging the derived theoretical framework with dispersion engineering methods known from state preparation, thus paving the way for real-world applications, the performance of which is investigated in section 6. Here, we introduce realistic experimental parameters for our waveguide devices and demonstrate the capability to fully control the pulse-mode structure of ultrafast pulsed quantum states of light. Finally, in section 7, we highlight the most important results of this work, and end with an outlook on the use of QPG and QPS in continuous variable quantum information processing.

2. Introduction

In recent years, different approaches have been introduced to prepare and manipulate ultrafast pulsed quantum states of light. One of the most common sources for the generation of photonics quantum states is parametric down-conversion (PDC) in nonlinear crystals. This is mainly due to the rather simple experimental implementation of PDC sources and their ability to achieve high photon-pair generation rates. When pumped by ultrafast pulses, PDC processes generate pulsed bi-photons with broad spectra. However, these states are usually highly correlated due to the constraints imposed by energy and momentum conservation [5, 6]. Hence, photon pairs are typically emitted into many inter- and intra-correlated spatial-spectral modes, the exact structure of which can be retrieved by applying a Schmidt decomposition to the biphoton amplitude distribution [7]. Upon the detection of one of the photons, the other one is projected onto a mixed state of all possible modes, rendering it ill-suited to linear optical quantum computation applications [8]. The common way of overcoming this limitation has been to use narrow-band spectral filtering to force the photons into one optical mode [9, 10]. However, this approach prohibitively lowers the photon generation rate as most of the generated signal is lost in the filtering process. It is thus not feasible in the case of large-scale quantum information applications [8]. In addition, only in the limit of infinitely narrow filtering one monochromatic, temporally de-localized mode is selected, and the photon's pulse characteristic is lost.

2.1. Preparation of ultrafast pulsed quantum states with waveguides

Recently, two new developments have made it possible to tackle the aforementioned problems. The use of integrated waveguide sources has a major impact on the structure of PDC photon pair states. In a bulk crystal, the generated photons are emitted at the natural phase-matching angles. This poses two problems. Firstly, the collection of photons pairs is experimentally challenging and typically inefficient. Secondly, the pump field always couples to an infinite

IOP Institute of Physics ⬦ DEUTSCHE PHYSIKALISCHE GESELLSCHAFT

number of spectral–spatially correlated modes, and thus the probability of creating a photon pair in one distinct mode becomes very low. In contrast, the emission in nonlinear waveguides is restricted to a well-defined set of discrete spatial modes defined by the waveguide, ideally allowing only the propagation of one individual mode in a single-mode waveguide[4]. It turns out that the probability of generating a photon pair in a distinct spatial mode is enhanced by several orders of magnitude [11, 12], since the total number of allowed modes is dramatically reduced inside the waveguide. Moreover, it also leads to an effective decoupling of the spatial from the spectral degree of freedom, since any spatial–spectral correlation necessitates more than one spatial mode. Even if other spatial modes apart from the ground mode are guided in the waveguide, modal waveguide dispersion usually ensures that both photons in those modes are created at different frequencies. Thus they can readily be removed by applying broadband spectral filters on the output state [13].

The second step on the way to achieving complete control over the modal structure of the generated quantum states of light is spectral source engineering. It has been proposed that by choosing adapted dispersion properties, photon pair generation can be tailored such that the signal and the idler are emitted into a single spectral pulse mode each [8, 14]. Later this was experimentally demonstrated for bulk crystal sources [15–17] and photonic crystal fibre sources [18–20]. Only recently has this been realized in a waveguided PDC source in a KTiOPO$_4$ crystal [21]. In this setup, the use of a waveguiding structure has led to an unprecedented brightness for sources of separable photon-pair states. Note that narrow-band spectral filtering is not necessary with these sources as the generation process itself only allows a single spectral pulse mode. Thus, the generated photon pairs are genuine quantum pulses and are completely separable, spectrally as well as spatially.

2.2. Manipulation of the pulse-mode structure of ultrafast quantum states

Until now, research on the manipulation of pulsed quantum states has mostly focused on shifting their central frequency. It has been shown that the sum-frequency generation (SFG) of single photons, in combination with subsequent photodetection, surpasses the efficiency of direct detection of near-infrared single photons [22–25]. Additionally, SFG has been proven to conserve the quantum characteristics of the input photon [26–28] and has already been utilized to implement measurement schemes with very high timing resolution, which overcomes the long integration times of current single-photon detectors [16]. Only last year, SFG was demonstrated for single-photon Fock states [29]. Note that recently also four-wave mixing in photonic crystal fibres has also been employed to demonstrate coherent frequency translation of single photons [30]. This highlights the broad interest in and numerous application possibilities for these techniques. With more and more single-photon sources available in the visible range, difference-frequency generation (DFG) has now attracted increasing interest. Recent experiments employ DFG to implement wavelength interfaces for quantum networks [31–33], which equivalently to the SFG process preserve the quantum characteristics of the input state.

Despite this considerable progress, the generation of ultrafast pulsed quantum states with a specific pulse-mode structure, be it the number of excited modes or their shape, has not been

---

[4] Here we only consider guided modes, neglecting any contributions that could be present due to phase-matched substrate modes. This simplification is justified, because the continuous distribution of substrate modes can be easily filtered out by spectral or spatial filters.
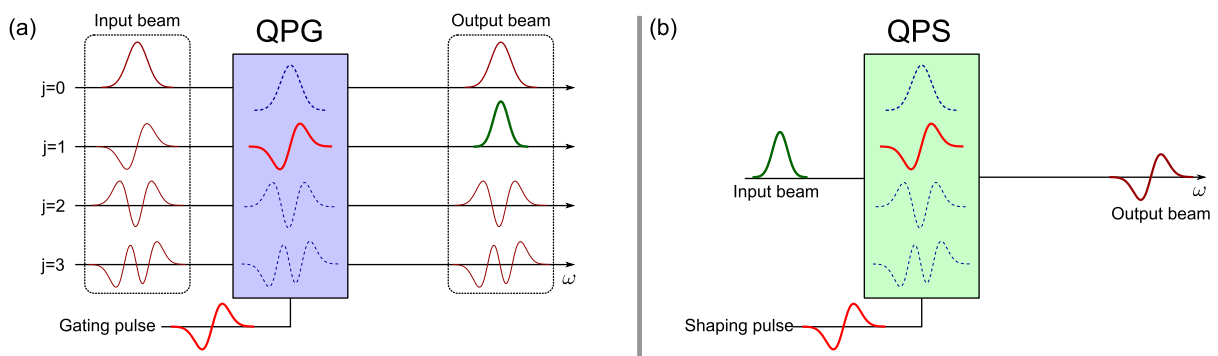
Figure 1. Schematic diagram of (a) a QPG and (b) a QPS. The QPG is based on an engineered ultrafast SFG in nonlinear optical waveguides. By shaping an ultrafast gating pulse, one specific pulse mode from a pulsed multimode input state is selected and shifted to another frequency. Then it can easily be split off while leaving the rest of the state untouched. The QPS is based on engineered ultrafast difference-frequency generation in nonlinear optical waveguides. An input pulse mode can be converted into an arbitrary output pulse mode by nonlinear interaction with an ultrafast shaping pulse. The output pulse mode's shape is given by the mode of the shaping pulse.

explored yet. Although the rich inherent mode structure of ultrafast optical quantum states is well known, before the QPG [4] there was no feasible way of controlling and manipulating the different modes separately.

2.3. Quantum pulse gate (QPG) and quantum pulse shaper (QPS)

We now combine findings from the field of quantum-state generation with techniques from state manipulation. Applying source engineering to frequency conversion reveals fascinating possibilities to achieve the desired goal of complete control over the pulse-mode structure of ultrafast quantum states. In [4], we have already proposed a QPG, a device based on engineered ultrafast SFG in nonlinear waveguides. This device enables us to address different inherent pulse modes of an ultrafast pulsed quantum state of light individually, as illustrated in figure 1(a). We would like to highlight that the QPG operation does not have any impact on the residual pulse-mode structure. This sets it apart from other experiments that focus on a direct manipulation of the spectral broadband-mode structure of ultrafast pulsed quantum states and that employ pulse shaping of photon-pair states [34–36]. This alternative approach also leads to highly interesting results for entanglement-based applications. Still, the manipulation is not pulse mode sensitive in the sense of accessing and separating out a single-mode quantum state with a specific temporal profile. In contrast, the QPG achieves mode selection by shaping an ultrafast, coherent gating pulse instead of the pulsed quantum state. The addressed mode is converted to the sum-frequency of the input pulse and gating pulse and is thus easily accessible. In addition, different orthogonal pulse modes can be interconverted into each other, rendering interference between them possible.

In this paper, we elaborate on the QPG concept and come up with another fundamental device, the QPS based on engineered ultrafast DFG. While the QPG addresses single pulse

IOP Institute of Physics **Φ** DEUTSCHE PHYSIKALISCHE GESELLSCHAFT

modes, the QPS enables us to convert an input quantum state with a Gaussian-shaped spectrum into a single-mode quantum state with arbitrary shape (see figure 1(b)). Here, an arbitrarily chosen pulse form of the coherent shaping pulse defines the output pulse mode. We would like to mention that a similar idea of shaping quantum pulses by means of frequency conversion with dispersion matching has been proposed in [37]. In contrast to this earlier work, we put special emphasis on the engineering of the dispersion characteristics of the nonlinear medium used, such that single-mode operation can be ensured, avoiding the insertion of any unwanted vacuum contributions.

Using QPG and QPS, pulsed quantum states can be generated and selected with unit efficiency in arbitrary pulse forms, and the encoding of quantum information in broadband mode basis and the successive read-out become possible. Therefore QPG and QPS will enable the implementation of quantum communication protocols, which exploit the rich pulse-mode structure of ultrafast states.

3. Linear transformations for sum-frequency generation (SFG) and difference-frequency generation (DFG) in comparison with parametric down-conversion

In this section, we qualitatively discuss the nonlinear three-wave mixing processes SFG, DFG and PDC, highlighting their formal similarities as well as examining their differences. In such a three-wave mixing process, three electrical fields interact inside a nonlinear medium, and the interaction Hamiltonian in the rotating-wave approximation is of the form

$$\hat{H}_{\text{int}} \propto \chi^{(2)} \int \mathrm{d}^3 r \, \hat{E}_{\text{a}}^{(+)}(\vec{r}, t) \hat{E}_{\text{b}}^{(-)}(\vec{r}, t) \hat{E}_{\text{c}}^{(-)}(\vec{r}, t) + \text{h.c.} \tag{1}$$

The $\hat{E}_i^{(+)}(\vec{r}, t)$ describe the positive frequency parts of the interacting electric fields and $\chi^{(2)}$ is the second-order nonlinearity of the medium. In PDC and single-photon SFG and DFG, two of the three fields are generally considered quantum mechanically. The remaining field is a bright, immutable pump field that can be treated classically. In this case, the interaction Hamiltonian becomes bilinear and Heisenberg's equation of motion yields linear input–output transformations for the creation and annihilation operators. Depending on which of the three fields is defined as a pump, one can distinguish between two flavours of processes that are characterized by different linear operator transformations.

This can be derived when considering a single-mode approximation to equation (1),

$$\hat{H}_{\text{int}} \propto \hat{a}\hat{b}^\dagger\hat{c}^\dagger + \hat{a}^\dagger\hat{b}\hat{c}. \tag{2}$$

Firstly, we assume that the field $E_{\text{a}}(\vec{r}, t)$ is the classical coherent pump field. We insert its classical amplitude α into the above equation and find that

$$\hat{H}_{\text{int}} \propto \alpha \, \hat{b}^\dagger\hat{c}^\dagger + \alpha^* \, \hat{b}\hat{c}. \tag{3}$$

The resulting operator formally corresponds to a two-mode squeezing operator (compare e.g. [38]), which means that this case describes PDC. Depending on the pump power of the bright field, either the photon pair characteristics (low-power regime) or the squeezer characteristics (high-power regime) dominate the PDC output state. The linear transformations between input and output operators evaluate to

$$\hat{b} \rightarrow \cosh(\zeta)\hat{b} - \sinh(\zeta)\hat{c}^\dagger, \tag{4}$$

$$\hat{c} \rightarrow -\sinh(\zeta)\hat{b}^\dagger + \cosh(\zeta)\hat{c}, \tag{5}$$
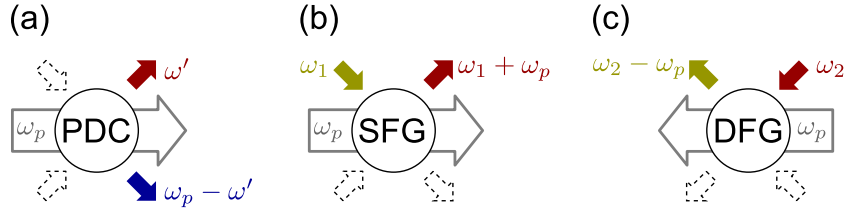
Figure 2. Schematic diagrams illustrating two different flavours of second-order nonlinear process. All processes are pumped by a classical undepleted field at a frequency ω_p, and the dashed arrows indicate vacuum modes. (a) In a PDC process, two photons are created and the evolution operator for this process is a two-mode squeezing operator. (b, c) In an SFG or DFG process, one incoming photon is annihilated and an outgoing photon at another frequency is created. Assuming that the frequencies involved in the two processes are equal, one can readily see that SFG and DFG are similar yet reversed processes, which is indicated in the schematics by the different directions that the arrows point to. The corresponding evolution operator for these processes is equivalent to a beamsplitter. For further details, see the text.

where the parameter ζ depends on the pump power and is related to the amount of squeezing in the generated pair state. This is discussed, for instance, in [39].

We find the other flavour of $\chi^{(2)}$ processes by assuming that the field $E_b(\vec{r}, t)$ corresponds to the pump field. We substitute its classical amplitude β in (2) and obtain

$$\hat{H}_{\text{int}} \propto \beta \, \hat{a}\hat{c}^\dagger + \beta^* \, \hat{a}^\dagger\hat{c}. \tag{6}$$

This expression is formally equivalent to an optical beamsplitter Hamiltonian and we can use the well-known beamsplitter input/output transformations for the operators $\hat{a}$ and $\hat{c}$,

$$\hat{a} \rightarrow \cos(\theta)\hat{a} - \mathrm{i}\sin(\theta)\hat{c}, \tag{7}$$

$$\hat{c} \rightarrow -\mathrm{i}\sin(\theta)\hat{a} + \cos(\theta)\hat{c}. \tag{8}$$

We identify θ with the beamsplitter angle, which depends on the pump power and the strength of the nonlinear interaction. This will be discussed later in great detail. We interpret this $\chi^{(2)}$-process as a beamsplitter that diverts optical beams into different frequency output ports depending on their initial frequency. Note that in single-photon quantum optics, this Hamiltonian describes SFG as well as DFG. In classical nonlinear optics, however, DFG is understood as a stimulated process. The bright pump field has the highest frequency and the process is seeded with a weak input field, which is enhanced through continuous conversion of pump photons. In that case, operator transformations similar to those for PDC are valid and the process could also be interpreted as seeded PDC. In contrast, we assume a single (or a few)-photon input state, which has the highest frequency and the 'seed' field is the bright field. By pinning the pump field to a fixed value in our process model, we exclude that stimulation can occur and the process becomes formally equivalent to SFG. Note that the usual no-pump-*depletion* approximation ($\partial E_p/\partial z = 0$) needs to be interpreted as a no-pump-*enhancement* approximation in this case. These findings are shown schematically in figure 2.

We move on to the derivation of the interaction Hamiltonian for quantum mechanical frequency conversion inside an optical waveguide.

4. Quantitative derivation of the SFG and DFG interaction Hamiltonian

4.1. Spatial mode considerations in a monochromatic approach

The interaction Hamiltonian of a frequency conversion process can be expressed as

$$\hat{H}_{\text{int}} = -d_{\text{eff}}\varepsilon_0 \int \mathrm{d}^3r\, E_{\text{p}}(\vec{r}, t)\hat{E}_{\text{i}}^{(+)}(\vec{r}, t)\hat{E}_{\text{o}}^{(-)}(\vec{r}, t) + \text{h.c.}, \tag{9}$$

where d_{eff} denotes the effective nonlinearity, E_{p} is the classical pump field, and $\hat{E}_{\text{i}}^{(+)}$ and $\hat{E}_{\text{o}}^{(-)}$ denote the operator expressions for the input signal and the converted output, respectively. As the interaction happens inside a nonlinear optical waveguide, the propagation of the fields is restricted to one direction, which is given by the waveguide axis and which we define as the z-direction. The ultrafast pump field then reads

$$E_{\text{p}}(\vec{r}, t) = A_{\text{p}}f_{\text{p}}(x, y)\int \mathrm{d}\omega_{\text{p}}\alpha(\omega_{\text{p}})\mathrm{e}^{-\mathrm{i}\omega_{\text{p}}t+\mathrm{i}\beta_{\text{p}}z}. \tag{10}$$

Here, $\alpha(\omega_{\text{p}})$ is the normalized spectral amplitude of the pump. The function $f_{\text{p}}(x, y)$ describes the transverse spatial distribution of the pump field with $\int \mathrm{d}^2r\,|f_{\text{p}}(x, y)|^2 = 1$ and β_{p} is the propagation constant of the corresponding transverse mode. By requiring that the area integration over the field intensity $I = \frac{1}{2}c\,n_{\text{p}}\varepsilon_0|E|^2$, where n_{p} denotes the refractive index at the pump frequency, corresponds to a power, we find that the amplitude A_{p} is related to the average pump pulse peak power P_{p} by

$$A_{\text{p}} = \left(\frac{2P_{\text{p}}}{c\,\varepsilon_0 n_{\text{p}}(\omega_{\text{p}})|\int \mathrm{d}\omega_{\text{p}}\alpha(\omega_{\text{p}})|^2}\right)^{1/2}. \tag{11}$$

We implicitly make use of the slowly varying envelope approximation in this calculation, which is valid as we consider only pulses with $\Delta\omega \ll \omega_0$. This also means that we can neglect the frequency dependence of the propagation constant β_{p} in (10).

To derive expressions for the quantized fields in a nonlinear waveguide, we start from the electric field operator for a propagating field in a dielectric with finite cross-section area $\mathcal{A}$, given in [40]. Note that we assume the wavevector components k_x and k_y of the quantum field to have fixed, finite values.

$$\hat{E}^{(+)}(x, y, z, t) = \mathrm{i}\int \mathrm{d}\omega\left(\frac{\hbar\omega}{4\pi\varepsilon_0 c\,n(\omega)\mathcal{A}}\right)^{1/2}\hat{a}(\omega)\mathrm{e}^{-\mathrm{i}\omega t+\mathrm{i}(k_x x+k_y y+k_z z)}. \tag{12}$$

In a nonlinear waveguide with field propagation along the z-direction, the solution of the Helmholtz equation yields a discrete spectrum of valid propagation constants $\beta_{mn} = k_z^{(mn)}$ and a set of allowed, localized transverse modes $\{f_{mn}(x, y)\}$, determined by the boundary conditions of the guiding geometry. The indices m and n denote the order of the transverse mode in the x- and y-directions. Each β_{mn} corresponds to exactly one mode and, in the case of a symmetric situation, the β_{mn} for the corresponding modes (e.g. β_{01} and β_{10}) become degenerate. For better readability, we only use one index m to describe the modes. The spatial localization of the fields implies continuous spectra of the individual wavevector components $k_x^{(m)}$ and $k_y^{(m)}$, given by $\tilde{f}_m(k_x, k_y) = \mathcal{FT}[f_m(x, y)]$.[5] The electric field inside a nonlinear waveguide is accordingly

---

[5] We deploy the symmetric definition of the Fourier transform, that is, $\tilde{f}(k) = \frac{1}{\sqrt{2\pi}}\int \mathrm{d}x\,f(x)\mathrm{e}^{-\mathrm{i}kx}$ and accordingly $f(x) = \frac{1}{\sqrt{2\pi}}\int \mathrm{d}k\,\tilde{f}(k)\mathrm{e}^{\mathrm{i}kx}$.

comprised of a superposition of quantum fields of the form given in (12), each corresponding to a single propagation direction. Summing over the transverse waveguide modes and integrating over $k_x^{(m)}$ and $k_y^{(m)}$, we find that

$$\hat{E}^{(+)}(x, y, z, t) = i \sum_m \int d\omega \left(\frac{\hbar \omega}{4\pi \varepsilon_0 c \, n_m(\omega)} \right)^{1/2} \hat{a}_m(\omega) e^{-i\omega t + i\beta_m z}$$

$$\times \int dk_x^{(m)} \, dk_y^{(m)} \, \tilde{f}_m(k_x, k_y) e^{i k_x^{(m)} x + i k_y^{(m)} y}. \tag{13}$$

This can—due to the Fourier relationship between position and momentum—be written as

$$\hat{E}^{(+)}(x, y, z, t) = i \sum_m 2\pi f_m(x, y) \int d\omega \left(\frac{\hbar \omega}{4\pi \varepsilon_0 c \, n_m(\omega)} \right)^{1/2} \hat{a}_m(\omega) e^{-i\omega t + i\beta_m z}. \tag{14}$$

We would like to point out that we account for the cross-sectional area by the spatial distributions $f_m(x, y)$, which are normalized such that $\int dx \, dy |f_m(x, y)|^2 = 1$ and which have units of inverse metres. Moreover, we assume that within the frequency range of the considered fields the variation in the spatial properties is negligible, due to the narrow-band approximation $\Delta\omega \ll \omega_0$. We substitute the electric field operators into (9) and rephrase the interaction Hamiltonian for single-photon frequency conversion as

$$\hat{H}_{\text{int}} = \frac{d_{\text{eff}} \hbar \pi}{c} A_p \sum_{l,m} \sqrt{\frac{\omega_i \omega_o}{n_{i,l} n_{o,m}}} \int dx \, dy f_p(x, y) f_{i,l}(x, y) f_{o,m}^*(x, y) \int dz \, e^{i(\beta_p \pm \beta_{i,l} \mp \beta_{o,m})z}$$

$$\times \int d\omega_p \, d\omega_i \, d\omega_o \alpha(\omega_p) e^{-i(\omega_p \pm \omega_i \mp \omega_o)t} \hat{a}_l(\omega_i) \hat{c}_m^\dagger(\omega_o) + \text{h.c.}, \tag{15}$$

where we discriminate between SFG and DFG. Here, labels i and o denote input and output fields, whereas indices *l* and *m* describe the transverse spatial modes of input and output fields respectively.

Now we move on to the calculation of the time evolution of the input quantum state during the conversion process. Note that the interaction of the Hamilton operator of equation (15) is time dependent and thus the exact solution has to take into account time-ordering effects. Here we present an approximate solution that neglects time-ordering effects, in order to emphasize the conceptual structure and to illustrate the main idea. In the appendix, we validate this approach by comparing the approximate solution with rigorous calculations we performed. We find that the shape of the mode functions does not change significantly when taking into account time ordering, but the maximum conversion efficiency drops to 90%. Still, these findings confirm that the analytical solution leads to reasonable results and can safely be applied. Hence, we write the time evolution of the quantum state during the conversion process

$$|\psi\rangle_{\text{out}} = \hat{U}(t)|\psi\rangle_0 = \exp\left(-\frac{i}{\hbar} \int dt \, \hat{H}_{\text{int}}(t) \right) |\psi\rangle_0. \tag{16}$$

Thus, we need to perform a time integration of the interaction Hamiltonian given in (15). This is a well-known procedure discussed, for PDC, in great detail in [8]. We only present the result

here, as the calculation, including the waveguide aspects, is straightforward,

$$\int dt \, \hat{H}_{\text{int}}(t) = \frac{2d_{\text{eff}}\hbar\pi^2}{c} A_{\text{p}} L \sum_{l,m} \sqrt{\frac{\omega_{\text{i}}\omega_{\text{o}}}{n_{\text{i},l}n_{\text{o},m}}} \frac{1}{\sqrt{A_{l,m}^{(\text{eff})}}} \int d\omega_{\text{i}} \, d\omega_{\text{o}} \alpha(\omega_{\text{io}})\phi_{l,m}(\omega_{\text{i}}, \omega_{\text{o}})\hat{a}_l(\omega_{\text{i}})\hat{c}^{\dagger}{}_m(\omega_{\text{o}}) + \text{h.c.}$$

(17)

Here, L is the length of the nonlinear waveguide. The function $\alpha(\omega_{\text{io}})$ is the spectral pump distribution defined as $\alpha(\omega_{\text{o}} - \omega_{\text{i}})$ for SFG and $\alpha(\omega_{\text{i}} - \omega_{\text{o}})$ for DFG, respectively, whereas the function $\phi_{l,m}(\omega_{\text{i}}, \omega_{\text{o}})$ characterizes the phase-matching and is given by

$$\phi_{l,m}(\omega_{\text{i}}, \omega_{\text{o}}) = \text{sinc}\left(\frac{\Delta\beta_{l,m}L}{2}\right) \approx \exp\left[-0.193 \cdot \left(\frac{\Delta\beta_{l,m}L}{2}\right)^2\right].$$

(18)

The expression $\Delta\beta_{l,m}$ describes the phase-mismatch of the propagation constants and evaluates to $\Delta\beta_{l,m} = \beta_{\text{p}} + \beta_{\text{i},l} - \beta_{\text{o},m} - \frac{2\pi}{\Lambda}$ for SFG and $\Delta\beta_{l,m} = \beta_{\text{p}} - \beta_{\text{i},l} + \beta_{\text{o},m} - \frac{2\pi}{\Lambda}$ for DFG, respectively. Finally, Λ is an optional poling period for quasi-phase-matching inside the waveguide. Following the usual conventions, we define an effective interaction area $A_{l,m}^{(\text{eff})}$,

$$\frac{1}{A_{l,m}^{(\text{eff})}} := \left[\int dx \, dy \, f_{\text{p}}(x, y) f_{\text{i},l}(x, y) f_{\text{o},m}^*(x, y)\right]^2.$$

(19)

Note that this should not be mistaken as a geometric area defined, for instance, by the waveguide cross-section. Instead it describes the overlap of the transverse spatial modes of the three interacting fields inside the nonlinear waveguide. This result also implies that simply using a smaller waveguide—while not changing the modal overlap characteristics—will not alter $A^{(\text{eff})}$ and will therefore not have any impact on the efficiencies of the processes. The product of pump distribution and phase-matching function is conveniently defined as the joint spectral distribution function,

$$G_{l,m}(\omega_{\text{i}}, \omega_{\text{o}}) = \frac{1}{N_{l,m}}\alpha(\omega_{\text{io}})\phi_{l,m}(\omega_{\text{i}}, \omega_{\text{o}}),$$

(20)

which describes the mapping between input and output frequencies for a specific pair of spatial modes l, m. The normalization factor $N_{l,m}$ reads $(\int d\omega_{\text{i}} \, d\omega_{\text{o}} |\alpha(_{\text{io}})\phi_{l,m}(\omega_{\text{i}}, \omega_{\text{o}})|^2)^{1/2}$.

4.2. Broadband pulse mode picture

The description derived so far has been in terms of monochromatic creation and annihilation operators. However, since we concentrate on $\chi^{(2)}$-interactions between ultrafast pulses, a much more natural approach is to consider broadband pulse modes. A suitable pulse-mode basis is found by applying a Schmidt decomposition to the joint spectral distribution function,

$$G_{l,m}(\omega_{\text{i}}, \omega_{\text{o}}) = \sum_j \kappa_j^{(l,m)}\varphi_j^{(l,m)}(\omega_{\text{i}})\psi_j^{(l,m)}(\omega_{\text{o}}).$$

(21)

Equation (21) yields two correlated sets of orthonormal broadband pulse-mode functions $\{\varphi^{(l,m)}(\omega_{\text{i}})\}$ and $\{\psi^{(l,m)}(\omega_{\text{o}})\}$. The diagonal values $\kappa_j^{(l,m)}$ are the real and positive Schmidt coefficients and satisfy $\sum_j (\kappa_j^{(l,m)})^2 = 1$. It is well known, for PDC, that the basis sets of the Schmidt decomposition, and thus the modal structure of the photons, are uniquely defined [2].

The same argument can also be applied here in the context of SFG and DFG. As for PDC, we define broadband creation and annihilation operators,

$$\hat{A}_{j,l,m} = \int d\omega_i \, \varphi_j^{(l,m)}(\omega_i)\hat{a}_l(\omega_i), \tag{22}$$

$$\hat{C}_{j,l,m} = \int d\omega_o \, \psi_j^{(l,m)}(\omega_o)\hat{c}_m(\omega_o). \tag{23}$$

Substituting those, we rewrite the expression for the time-integrated interaction Hamiltonian from (17), and arrive at the broadband pulse-mode picture,

$$\int dt\, \hat{H}_{int}(t) = \frac{2d_{eff}\hbar\pi^2}{c}A_p L \sum_{l,m}\sqrt{\frac{\omega_i\omega_o}{n_{i,l}n_{o,m}}}\frac{N_{l,m}}{\sqrt{A_{l,m}^{(eff)}}}\sum_j (\kappa_j^{(l,m)}\hat{A}_{j,l,m}\hat{C}_{j,l,m}^\dagger + h.c.)$$

$$= \hbar\sum_{l,m}\sum_j \theta_{j,l,m}(\hat{A}_{j,l,m}\hat{C}_{j,l,m}^\dagger + \hat{A}_{j,l,m}^\dagger\hat{C}_{j,l,m}). \tag{24}$$

By introducing the effective coupling constant $\theta_{j,l,m}$ into (24), we reveal the simple beamsplitter structure of the Hamiltonian [41], as already announced in (6). In contrast to a conventional beamsplitter, however, this Hamiltonian does not couple two k-modes (or beam paths), but rather two broadband pulse modes $\hat{A}_{j,l,m}$ and $\hat{C}_{j,l,m}$ at different frequencies! This is a unique feature of ultrafast frequency conversion processes and makes them ideal candidates for the implementation of the QPG and QPS.

5. Pushing towards applications

5.1. General non-engineered SFG and DFG

QPG and QPS are unique in their single-mode operation on broadband pulse modes. In this section, we discuss the implementation of genuine QPG or QPS in a feasible experimental setup. We restrict the analysis to only one pair of transverse spatial modes (l, m), which simplifies the notation but does not change the underlying physics. In the experimental setting, the selection of one spatial mode can be accomplished by broadband spectral filtering [13]. In this case, the time-integrated, effective SFG and DFG Hamiltonian from (24) reads

$$\int dt\, \hat{H}_{int}(t) = \hbar\sum_j \theta_j(\hat{A}_j\hat{C}_j^\dagger + \hat{A}_j^\dagger\hat{C}_j), \tag{25}$$

with the broadband operators defined as

$$\hat{A}_j = \int d\omega_i \, \varphi_j(\omega_i)\hat{a}(\omega_i), \tag{26}$$

$$\hat{C}_j = \int d\omega_o \, \psi_j(\omega_o)\hat{c}(\omega_o). \tag{27}$$

The complete, orthonormal function sets $\{\varphi_j(\omega_i)\}$ and $\{\psi_j(\omega_o)\}$ represent the intrinsic pulse-mode structure of the SFG or DFG processes, obtained from the Schmidt decomposition of the joint spectral distribution function $G(\omega_i, \omega_o) = \alpha(\omega_{io})\phi(\omega_i, \omega_o)$. On the one hand, these are determined by the pump pulse characteristics, but on the other hand they also depend
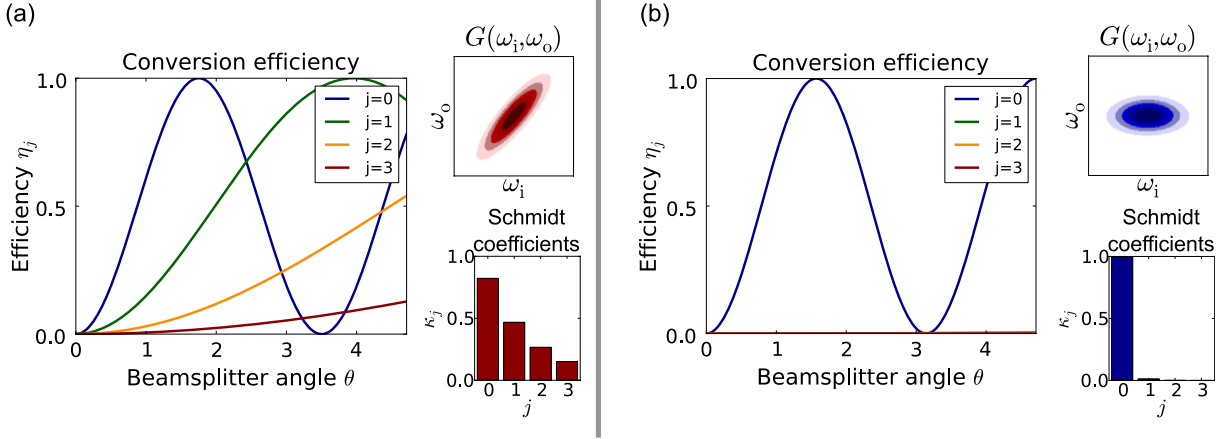
Figure 3. Conversion efficiencies η_j, joint spectral distribution functions $G(\omega_i, \omega_o)$ and Schmidt coefficients κ_j for the first four pairs of pulse modes ($j = 0, \ldots, 3$). (a) Non-engineered process with several $\kappa_j \neq 0$. For a given overall beamsplitter angle θ, all modes are converted to a certain extent given by $\eta_j = \sin(\kappa_j \cdot \theta)^2$. However, an overall unit efficiency can generally not be accomplished. (b) Source-engineered process with one predominant $\kappa_j \approx 1$. By choosing an appropriate θ, pulse mode $\varphi(\omega_i)$ can be converted into pulse mode $\psi(\omega_o)$ with unit efficiency, allowing for QPG operation.

critically on the nonlinear waveguide's material and modal dispersion properties. We have already stressed the formal equivalence between the expression from (25) and a sum of optical beamsplitter Hamiltonians. Hence the linear transformation for the broadband operators can be readily written as

$$\hat{A}_j \rightarrow \cos(\theta_j)\hat{A}_j - \mathrm{i} \sin(\theta_j)\hat{C}_j, \tag{28}$$

corresponding to a pulse mode conversion between $\varphi_j(\omega_i)$ and $\psi_j(\omega_o)$ with efficiency $\eta_j = \sin^2(\theta_j)$. According to (24), the coupling constant θ_j is given by

$$\theta_j = \kappa_j \cdot \frac{2d_{\mathrm{eff}}\pi^2 LN}{c} \sqrt{\frac{2\omega_i\omega_o}{c\,\varepsilon_0 n_p n_i n_o |\int \mathrm{d}\omega_p \alpha(\omega_p)|^2}} \sqrt{\frac{P_p}{A^{(\mathrm{eff})}}} = \kappa_j \cdot \theta. \tag{29}$$

Here, θ is an overall beamsplitter angle defined by the process parameters. Its impact on the different modes j is given by θ_j, where, for each mode, the overall beamsplitter angle is weighted with the corresponding Schmidt coefficient κ_j. In figure 3(a), we illustrate a general, non-engineered SFG. We show the joint spectral distribution function $G(\omega_i, \omega_o)$ as well as the Schmidt coefficients κ_j for the first four pairs of pulse modes and plot the conversion efficiencies η_j versus the beamsplitter angle θ. It is obvious that for any given value of θ, all pulse modes with $\kappa_j \neq 0$ are converted to a certain extent. Yet, in general, single-mode operation is not achievable, nor can conversion with $\eta_j = 1$ for different pulse modes simultaneously be accomplished. We note an exception to this rule: under certain conditions (e.g. a cw pump), input and output modes are perfectly correlated. Then all κ_j share the same value and all modes are converted with the same efficiency. The process is then highly multimode but the overall efficiency can reach unity for high pump powers.

5.2. Source-engineered SFG and DFG: towards genuine QPG and QPS

We have shown that SFG and DFG in general are multimode processes. But for QPG and QPS we require single-mode operation in order to avoid the signal degradation introduced by vacuum contributions and to achieve unit efficiency. Reducing the intrinsic pulse-mode structure of a $\chi^{(2)}$-nonlinear process to only one pair of modes has been extensively studied in PDC, where source engineering led to the desired results [8, 15, 16]. Experimentally, this is accomplished by group-velocity matching inside the nonlinear medium. If the pump and either the signal or the idler share the same group velocity, the phase-matching function becomes parallel to one of the axes when plotted in an (ω_s, ω_i)-diagram. Then, the Schmidt decomposition yields—given that the process is pumped by an ultrafast pump—only one pair of pulse modes that is excited with unit efficiency.

We transfer this insight to our analysis of SFG and DFG and employ it for spectral engineering of the conversion. The time-integrated Hamiltonian from (25) for our special case reduces to

$$\int \mathrm{d}t\, \hat{H}_{\mathrm{int}} = \hbar\theta(\hat{A}\hat{C}^{\dagger} + \hat{A}^{\dagger}\hat{C}) \tag{30}$$

and can be interpreted as a beamsplitter operating on only one pair of pulse modes $\varphi(\omega_i)$ and $\psi(\omega_o)$. As an example, we show an engineered case in figure 3(b), where pump and input signals are group-velocity matched. Note that, in contrast to the previous non-engineered case, the joint spectral distribution function now shows no spectral correlations between input and output frequencies; that is, it is oriented along the axes of the diagram. As in PDC, this is a direct consequence of the horizontally oriented phase-matching function and thus of the group-velocity matching. The distribution of κ_j reveals that only one coefficient, κ_0, differs significantly from zero. This is also reflected in the plot of the conversion efficiencies. Only a single pulse mode is addressed and, by choosing $\theta = \frac{\pi}{2}$, converted with unit efficiency, and no vacuum is coupled into the signal beam. Hence we find that by group-velocity matching the pump and either the input or the output, we can achieve genuine single-mode operation and therefore implement QPG and QPS. Note that the data in figure 3 have been calculated using our modelling and realistic experimental parameters, which are specified in section 6.

Knowing how to achieve single-mode operation of SFG and DFG, the next step is to investigate how we can exact complete control over the pulse modes $\varphi(\omega_i)$ and $\psi(\omega_o)$. A QPG selects a specific pulse mode from an input state and a QPS generates an arbitrary pulse mode from a Gaussian input mode. Hence, for QPG we require control over $\varphi(\omega_i)$, whereas for QPS we require the shaping of $\psi(\omega_o)$, respectively. In figures 4(a)–(c), we consider QPG. Shown are the phase-matching and pump functions as well as the resulting joint spectral distribution function. Note that the axes are given wavelength units rather than frequency for convenience. We find that the output mode $\psi(\omega_o)$ is defined solely by the phase-matching. We performed calculations for three different spectral shapes of the pump and it is obvious that the input mode $\varphi(\omega_i)$ has the form of the respective pump mode. Thus, in a QPG, spectrally shaping the bright gating pulse leads to the selection of an arbitrary pulse mode. In contrast, figures 4(d)–(f) illustrate the situation for QPS. Now, the pump and the output are group-velocity matched, causing a vertical phase-matching function. Again we calculated three different spectral pump distributions. We find that the spectral shape of the pump now defines the output mode $\psi(\omega_o)$ of the QPS and the input mode $\varphi(\omega_i)$ is fixed by the phase-matching. Summing up these findings,
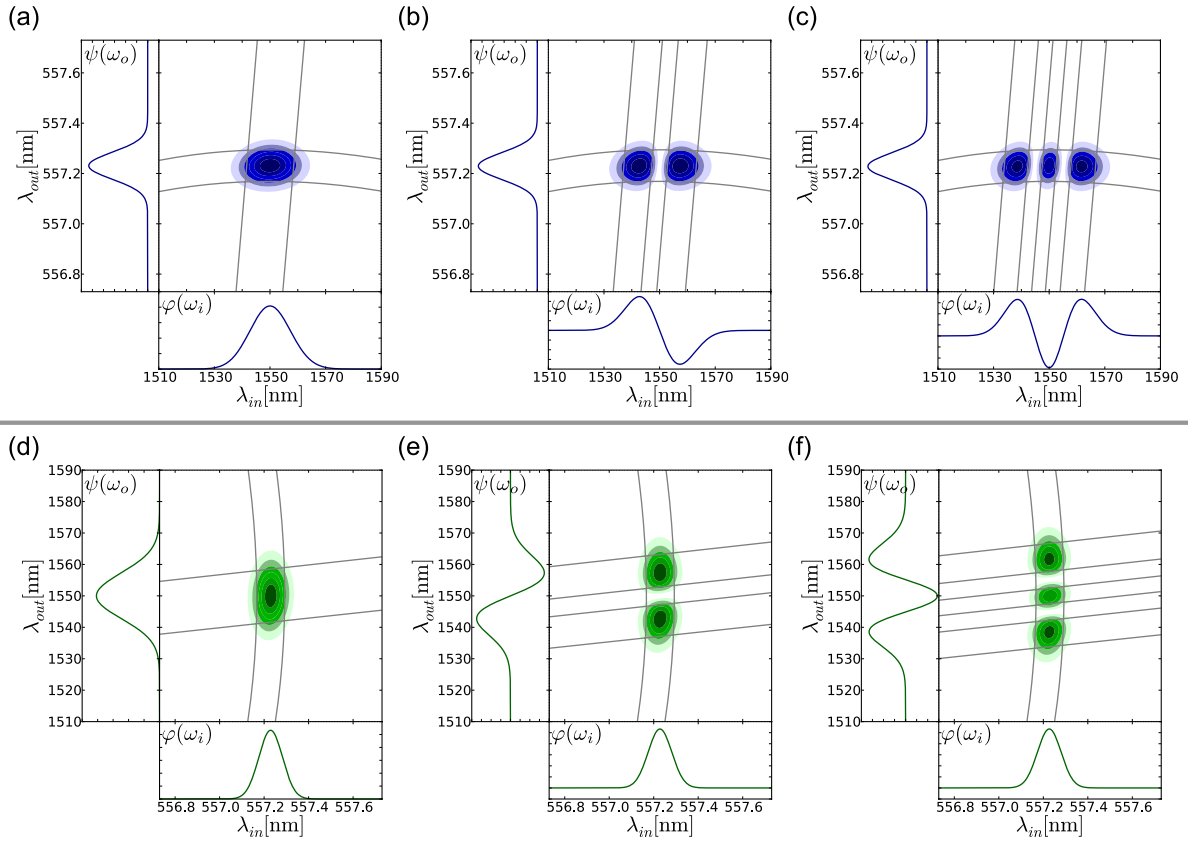
Figure 4. Joint spectral distribution, pump and phase-matching function as well as pulse modes $\varphi(\omega_i)$ and $\psi(\omega_o)$ for QPG (a–c) and QPS (d–f). Note that the functions are plotted against wavelengths for reasons of convenience. In a QPG, the intrinsic pulse mode $\varphi(\omega_i)$ can be manipulated by shaping the bright gating pulse, whereas the pulse mode $\psi(\omega_o)$ is fixed by the phase-matching function. Therefore, arbitrary input modes are mapped to the same output mode, allowing for interference of formerly orthogonal modes. In contrast, in a QPS, shaping the bright pulse defines the output pulse mode $\psi(\omega_o)$. The input pulse mode is now defined by the phase-matching function. Thus, an arbitrary mode can be generated from an input that is matched to $\varphi(\omega_i)$. The data presented here are calculated using realistic experimental parameters, as specified in section 6.

we end up with the following correspondences,

$$\alpha(\omega_p) \to \varphi(\omega_i), \quad \phi(\omega_i, \omega_o) \to \psi(\omega_o) \quad \text{for QPG}, \tag{31}$$

$$\phi(\omega_i, \omega_o) \to \varphi(\omega_i), \quad \alpha(\omega_p) \to \psi(\omega_o) \quad \text{for QPS}. \tag{32}$$

We have demonstrated that we can achieve complete control over the required pulse mode of the QPG or QPS by shaping the bright gating pulse or shaping pulse, respectively. Note, however, that we considered only the intrinsic modes of the QPG and QPS, which do not necessarily have to coincide with the pulse-mode structure of an input signal.
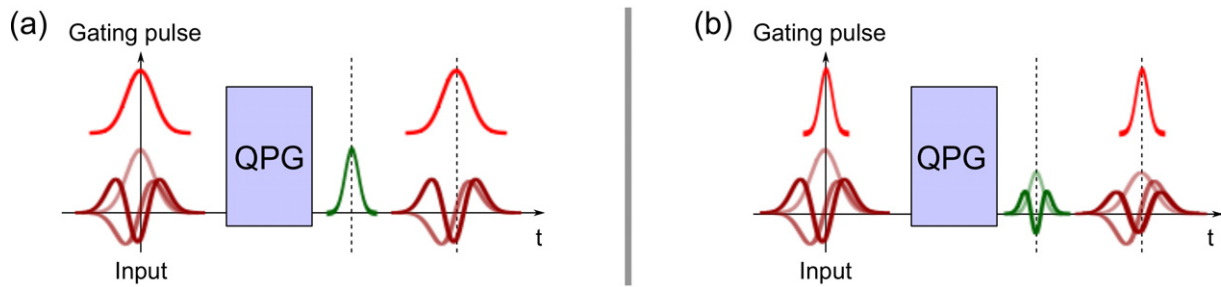
Figure 5. (a) Mode-matched QPG. The bright gating pulse has the same duration as the input signal, leading to matching of the input pulse-mode structure and $\varphi(\omega_i)$ of the QPG. Only a single pulse mode of the input—the one that overlaps with $\varphi(\omega_i)$—is selected and converted with unit efficiency. (b) Mode-mismatch in a QPG. The gating pulse and input signal have different durations, leading to an overlap of $\varphi(\omega_i)$ with all input signal modes with the same parity. Hence, all of those modes are selected and converted to a certain degree. QPG operation is then not possible.

5.3. Mode matching a QPG or a QPS

Given a specific QPG or QPS, the input signal's pulse-mode structure must coincide with the pulse modes $\{\varphi(\omega_i)\}$ accepted by the device, in order to guarantee mode selectivity and high conversion efficiency. We first discuss this for the QPG. We have shown that the QPG can be easily adapted to a wide range of input signals by spectrally shaping the coherent gating pulse. The output mode $\psi(\omega_o)$ is solely defined by the phase-matching function and is independent of the pump pulse shape. It can typically be approximated by a Gaussian spectrum [8]. Hence any selected mode from an input state is mapped to the same output mode.

In figure 5(a), we illustrate this situation. The input signal and gating pulse share the same duration and the QPG is mode-matched to the input. Only the desired mode from the input signal is selected and converted with unit efficiency. In contrast, figure 5(b) demonstrates the impact of a mode mismatch on the QPG operation. The gating pulse duration significantly differs from the input pulse duration and the intrinsic QPG pulse mode $\varphi(\omega_i)$ overlaps with all signal modes of the same parity. We end up with a case similar to multimode SFG, with the only difference being that the diverse conversion efficiencies for the modes are due to the different overlaps between $\varphi(\omega_i)$ and the corresponding signal-state modes. Because an overall efficiency of unity cannot be achieved here and the process is not mode-selective anymore, it becomes clear that careful mode-matching is vital for a successful QPG implementation.

The situation is different for QPS: the phase-matching function is vertical in the (ω_i, ω_o)-plane (compare figures 4(c)–(f)) and the input mode $\varphi(\omega_i)$ is now defined by the phase-matching function alone. The QPS accepts only Gaussian input modes that are matched to $\varphi(\omega_i)$. However, shaping the bright pulse allows for defining the output mode $\psi(\omega_o)$, rendering it possible to generate any pulse mode from an input pulse with a Gaussian spectrum. If the input state is not matched to $\varphi(\omega_i)$, this does not change the spectral form of the output pulse. The drawback is that it is not the complete input that gets converted and vacuum contributions are introduced.

We note that the same physical nonlinear waveguide device could be used as QPG or QPS, depending on whether SFG or DFG is implemented: this shows that QPG and QPG can be
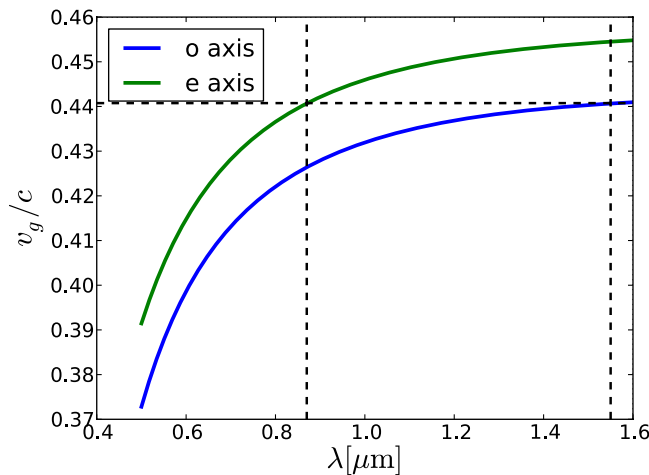
Figure 6. Group velocities of the fundamental waveguide modes in a Ti-indiffused PPLN waveguide. For a 1550 nm input oriented along the ordinary axis, an extraordinarily polarized pump pulse centred on 870 nm is group-velocity matched. For a QPG, this consequently leads to an output at 557 nm that has to be oriented along the ordinary axis. It becomes obvious that for a wide range of input signal wavelengths, group-velocity matched gating pulses can be found that still satisfy feasible experimental parameters.

seen as reverse operations of each other. The results illustrate that QPG and QPS are versatile tools that can be easily adapted to a large range of input and output states, making them highly flexible and appealing for many applications.

6. Performance of QPG and QPS considering realistic experimental parameters

We conclude our analysis demonstrating the experimental feasibility of a QPG and derive, with the help of the theoretical model outlined in sections 3–5, an expression for the pump power for maximally efficient operation. The results of the calculation apply to QPS as well, since both devices can be implemented in the same nonlinear waveguide. SFG phase-matching implies an existing DFG phase-matching; only the roles of input and output fields are interchanged. The coupling constant θ is the same for both processes. The bright pulse, used as a gating or shaping pulse depending on the application, will be called a pump in this paragraph for ease of reading. The input field is at 1550 nm and the third field is referred to as the output.

As a key point for the experimental setup, we require that it can be operated at 1550 nm. The constraint of group-velocity matching determines the pump wavelength as soon as the input wavelength gets fixed, which in turn then also defines the output wavelengths due to energy conservation. We assume that the conversion takes place in a Ti-indiffused PPLN waveguide with a length of $L = 10$ mm and at a temperature of $T = 190°$C to prevent the impact of photorefraction. The effective Sellmeier equations for the three participating fields were obtained by calculating the effective refractive indices of ordinary and extraordinary polarized fields with a finite-element method described in [42]. The effective equations were then fitted against the calculated values. Note that the following calculations are based on these effective Sellmeier equations.
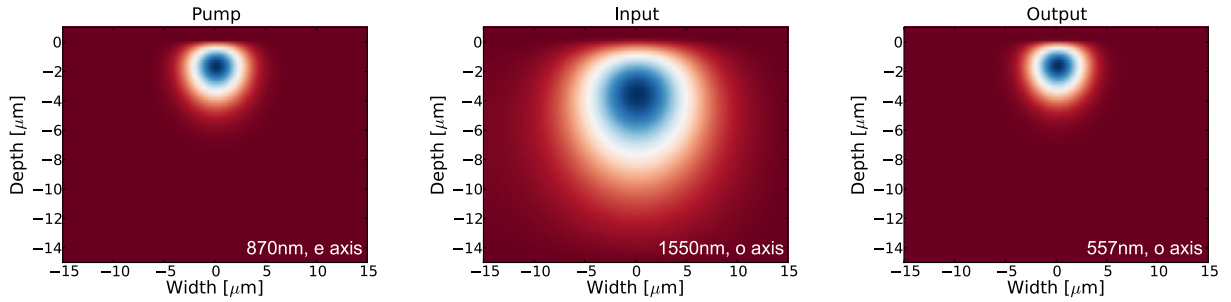
Figure 7. Transverse spatial mode profiles of the fundamental waveguide modes in a Ti-indiffused PPLN waveguide. The mode profiles were calculated using a finite elements method. The overlap between the pump and the output exceeds 99% because the guiding for ordinarily polarized fields is not as strongly pronounced as for extraordinarily polarized fields.

In figure 6, we plot the group velocities for the ordinary and extraordinary crystal axes and assume for our modelling that all fields propagate in the fundamental transverse waveguide mode. If the input light is ordinarily (TE-)polarized with a central wavelength of 1550 nm, we find that the group-velocity matched pump has to be extraordinarily (TM-) polarized and centred on 870 nm. The ordinarily polarized output is then at 557 nm. From figure 6, we can clearly recognize that a group-velocity matched pump can be found for any input, as long as the input is o-polarized. The effective refractive indices of the participating fields were calculated to be $n_p = 2.18$, $n_i = 2.21$ and $n_o = 2.32$ and we derive a periodic poling period of $\Lambda \approx 4.28\,\mu$m required for quasi-phase-matching inside the waveguide.

In figure 7, we plot the transverse spatial distributions of the input, pump and output modes, also obtained with the finite-element method from [42]. From these we calculate the effective interaction area $A^{(\text{eff})} \approx 64\,\mu\text{m}^2$. The conversion efficiency for a single-mode operation is $\eta = \sin^2(\theta)$ and the condition for unit efficiency can be specified by

$$\theta \overset{!}{=} \frac{\pi}{2}, \tag{33}$$

$$P_p \overset{!}{=} \left(\frac{c}{4\pi d_{\text{eff}} L N}\right)^2 \frac{c\,\varepsilon_0 n_p n_i n_o |\int \mathrm{d}\omega_p \alpha(\omega_p)|^2 A^{(\text{eff})}}{2\omega_i \omega_o}. \tag{34}$$

Assuming an input pulse duration of roughly 300 fs, we calculate a required pump peak power of $P_p \approx 22$ W for optimal conversion efficiency. If a pump laser system with a repetition frequency of 76 MHz is used, we obtain an average pump power of $P_{\text{av}} \approx 0.5$ mW inside the waveguide. This leads to required average pump powers of a few mW in front of the QPG or QPS, taking into account realistic waveguide coupling losses. These values are lower than formerly reported pump powers for similar experiments [22–24, 27, 29], owing to the careful source engineering that we applied to our process. This grants a significant advantage over experiments without spectrally engineered SFG, even though we employ a cross-polarized process with an effective nonlinearity that is lower by one order of magnitude than that of a process where all three fields are oriented along the extraordinary crystal axis.

7. Conclusion and outlook

In conclusion, we have presented a feasible way to achieve complete control over the pulse-mode structure of ultrafast pulsed quantum states of light. We combined findings from quantum state generation and techniques from state manipulation, by applying spectral-source engineering and integrated optics to frequency conversion of ultrafast single photons. We showed that single-mode ultrafast SFG and DFG in $\chi^{(2)}$-nonlinear materials are possible and analysed two highly flexible and versatile devices, namely QPG and QPS. The QPG is based on ultrafast SFG and offers the possibility of selecting arbitrary pulse modes from an ultrafast multimode input state. The selected mode gets converted with unit efficiency and is mapped onto a Gaussian output mode. The residual mode structure of the input is left intact, allowing for cascaded operation to convert multiple modes. As all input modes are mapped onto the same output mode, interference of formerly orthogonal states becomes possible. In contrast, the newly introduced QPS is based on DFG and implements the reverse operation of a QPG. It enables us to generate an arbitrary pulse form from a Gaussian input mode. The output mode is defined by a bright shaping pulse; thus highly flexible state preparation can be achieved. We have presented a quantitative analysis of QPG and QPS and derived feasible experimental parameters with which the proposed devices can be implemented, rendering them practical instead of merely conceptual.

As a final remark, we would like to point out that our analysis is in no way constrained to single-photon states. Although we consider single-photon input states, the introduced concepts can be generalized to classical and non-classical multi-photon states. In this framework, the use of QPG and QPS provides us with an attractive opportunity to successively select and spatially separate arbitrary pulse modes from a multimode input state while leaving the residual beam intact. Employing a series of QPGs operating on the same pulse mode in each arm of a multimode twin-beam squeezer source allows for a feasible implementation of non-Gaussian operations and thus constitutes an important step towards the realization of multimode continuous variable entanglement distillation. QPS, on the other hand, can be used to synthesize multimode continuous variable Gaussian states in a mode-by-mode fashion. The prepared states can then be transmitted as a bundle, since they do not interact with each other and since they all experience the same dispersion during transmission and therefore stay orthogonal. This paves the way for dense channel multiplexing in continuous variable quantum communication.

Acknowledgments

Appendix. Impact of time ordering

Since the interaction of the Hamilton operator of equation (15) is time dependent, it might be assumed that time-ordering effects have a major impact on the intrinsic mode structure of the process, in particular if a perturbative solution is not sufficient. This case is associated with unit conversion efficiency, needed for perfect QPG and QPS operation. In our analysis, we have nevertheless deployed the approximate solution that neglects time ordering. The impact of time ordering on the process of ultrafast PDC has been thoroughly investigated in [43], with the result
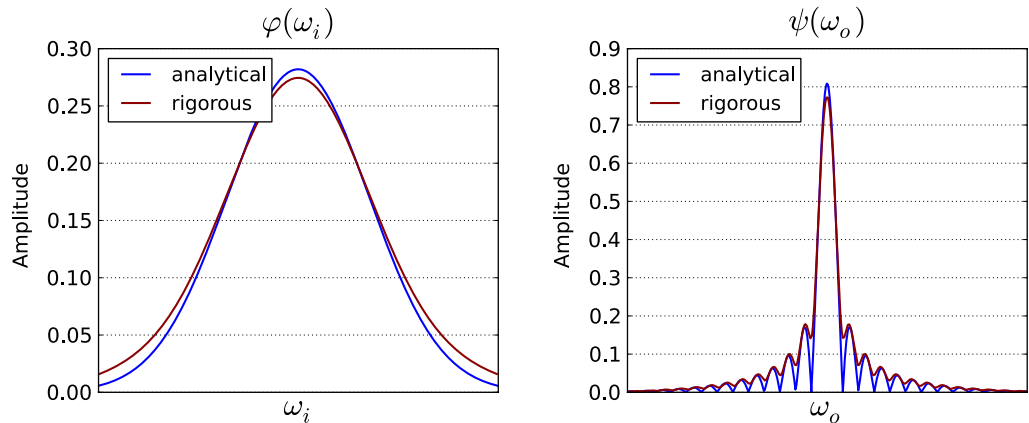
Figure A.1. Input modes $\varphi(\omega_i)$ as well as output modes $\psi(\omega_o)$ of the considered processes, obtained from the analytical solution (blue) and rigorous calculation (red), respectively. Obviously, time ordering has only a small impact on the actual mode shape. This can simply be corrected for in our schemes by adjusting the spectrum of the bright pump pulse. Note that the oscillations in the output modes originate from the sinc function that describes the phase matching.

that time ordering mostly affects the amplitudes but not the shapes of the intrinsic pulse modes. In [37], the authors actually study a three-wave mixing process and find in their numerical simulation no major discrepancy with their analytical solution. This already indicates that, at least for low conversion efficiencies where a perturbative solution is sufficient, time ordering can be neglected. However, since we aim at conversion efficiencies of unity and cannot conclude for sure that the above results remain valid in our case, we performed rigorous numerical simulations that take into account all time-ordering effects. Note that the results presented are all obtained for the case of maximum conversion efficiency. Additionally, the simulated processes are the ones discussed in this work. That is, the pump pulse and the input pulse are group-velocity matched and the processes have decorrelated joint spectral distribution functions, as is the case in figure 3(b).

Figure A.1 depicts the analytical as well as the rigorous input modes $\varphi_{\mathrm{ana}}(\omega_i)$ and $\varphi_{\mathrm{rig}}(\omega_i)$ and the corresponding output modes $\psi_{\mathrm{ana}}(\omega_o)$ and $\psi_{\mathrm{rig}}(\omega_o)$, respectively. It nicely illustrates that time ordering has only a slight impact on the shape of the modes, as expected from [43]. The change in the modes can easily be compensated for, in our proposed scheme, by adjusting the spectrum of the bright gating pulse. Note that the oscillations in the output modes originate from the sinc function that describes the phase-matching. These also cause the slight multi-modeness that can be seen in the Schmidt coefficients in figure A.2, where the first higher-order mode is also excited with a certain probability. Comparing again analytical and rigorous solutions, we find that time ordering slightly shifts the weights between the different modes. However, we want to note that no new modes occur in the process due to time ordering. The main difference is found when considering the maximum conversion efficiency. It turns out that this value drops in the rigorous solution to 90%, instead of the unit efficiency obtained with the analytical approach.

This behaviour will be thoroughly analysed in [44]. We want to stress here that all characteristics introduced by the side lobes of the sinc function can be washed out through careful design of the nonlinearity inside the waveguide, as shown in [45]. Therefore the device
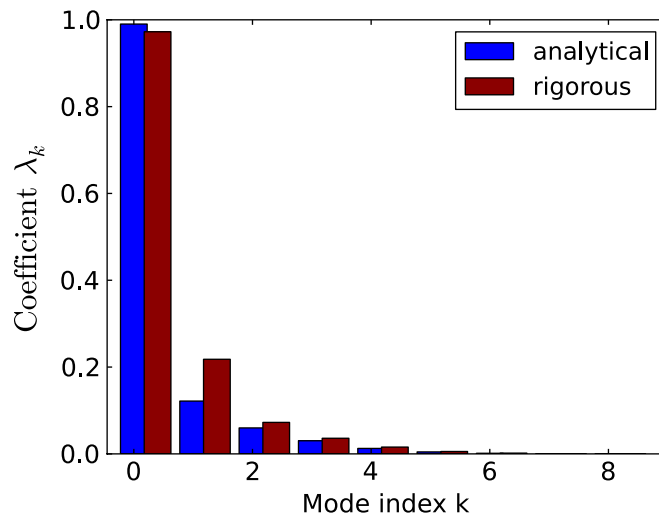
Figure A.2. Schmidt coefficients λ_k obtained from the analytical as well as the rigorous solution. Time ordering causes a slight shift in the excitation of the different modes. In addition, it leads to a drop in the maximum conversion efficiency to 90%, as compared with the unit conversion efficiency reached in the analytical solution.

performance calculated here only represents a lower bound and might be increased in the future, for instance by implementing a Gaussian-shaped phase-matching function.

In conclusion, we find by comparing analytical and numerical solutions that the assumption that time ordering can be neglected is, in fact, a rather good approximation, even for the cases of high conversion efficiencies analysed in this work.

References

[1] Titulaer U M and Glauber R J 1966 Density operators for coherent fields *Phys. Rev.* **145** 1041–50
[2] Martinelli M, Treps N, Ducci S, Gigan S, Maître A and Fabre C 2003 Experimental study of the spatial distribution of quantum correlations in a confocal optical parametric oscillator *Phys. Rev.* A **67** 023808
[3] Knill E, Laflamme R and Milburn G J A 2001 Scheme for efficient quantum computation with linear optics *Nature* **409** 46–52
[4] Eckstein A, Brecht B and Silberhorn C 2010 A quantum pulse gate based on spectrally engineered sum frequency generation arXiv:1007.3215
[5] Keller T E and Rubin M H 1997 Theory of two-photon entanglement for spontaneous parametric down-conversion driven by a narrow pump pulse *Phys. Rev.* A **56** 1534–41
[6] Grice W P, U'Ren A B and Walmsley I A 2001 Eliminating frequency and space-time correlations in multiphoton states *Phys. Rev.* A **64** 063815
[7] Law C K, Walmsley I A and Eberly J H 2000 Continuous frequency entanglement: effective finite hilbert space and entropy control *Phys. Rev. Lett.* **84** 5304–7
[8] U'Ren A B, Silberhorn C, Banaszek K, Walmsley I A, Erdmann R, Grice W P and Raymer M G 2005 Generation of pure-state single-photon wavepackets by conditional preparation based on spontaneous parametric downconversion *Laser Phys.* **15** 146–61
[9] de Riedmatten H, Marcikic I, Tittel W, Zbinden H and Gisin N 2003 Quantum interference with photon pairs created in spatially separated sources *Phys. Rev.* A **67** 022301

IOP Institute of Physics · DEUTSCHE PHYSIKALISCHE GESELLSCHAFT

[10] Kaltenbaek R, Blauensteiner B, Zukowski M, Aspelmeyer M and Zeilinger A 2006 Experimental interference of independent photons *Phys. Rev. Lett.* **96** 240502

[11] Tanzilli S, de Riedmatten H, Tittel W, Zbinden H, Baldi P, de Micheli M, Ostrowsky D B and Gisin N 2001 Highly efficient photon-pair source using periodically poled lithium niobate waveguide *Electron. Lett.* **37** 26–8

[12] Fiorentino M, Spillane S M, Beausoleil R G, Roberts T D, Battle P and Munro M W 2007 Spontaneous parametric down-conversion in periodically poled KTP waveguides and bulk crystals *Opt. Express* **15** 7479–88

[13] Mosley P J, Christ A, Eckstein A and Silberhorn C 2009 Direct measurement of the spatial-spectral structure of waveguided parametric downconversion *Phys. Rev. Lett.* **103** 233901

[14] Garay-Palmett K, Rangel-Rojo R and U'Ren A B 2009 Tailored photon pair preparation relying on full group velocity matching in fibre-based spontaneous four-wave mixing *J. Mod. Opt.* **56** 946

[15] Mosley P J, Lundeen J S, Smith B J, Wasylczyk P, U'Ren A B, Silberhorn C and Walmsley I A 2008 Heralded generation of ultrafast single photons in pure quantum states *Phys. Rev. Lett.* **100** 133601

[16] Kuzucu O, Wong F N C, Kurimura S and Tovstonog S 2008 Joint temporal density measurements for two-photon state chracterization *Phys. Rev. Lett.* **101** 153602

[17] Shi X, Valencia A, Hendrych M and Torres J 2008 Generation of indistinguishable and pure heralded single photons with tunable bandwidth *Opt. Lett.* **33** 875–7

[18] Cohen O, Lundeen J S, Smith B J, Puentes G, Mosley P J and Walmsley I A 2009 Tailored photon-pair generation in optical fibers *Phys. Rev. Lett.* **102** 123603

[19] Halder M, Fulconis J, Cemlyn B, Clark A, Xiong C, Wadsworth W J and Rarity J G 2009 Nonclassical 2-photon interference with separate intrinsically narrowband fibre sources. *Opt. Express* **17** 4670–6

[20] Söller C, Brecht B, Mosley P J, Zang L, Podlipensky A, Joly N Y, Russell P, St J and Silberhorn C 2010 Bridging visible and telecom wavelengths with a single-mode broadband photon pair source *Phys. Rev.* A **81** 031801

[21] Eckstein A, Christ A, Mosley P J and Silberhorn C 2011 Highly efficient single-pass source of pulsed single-mode twin beams of light *Phys. Rev. Lett.* **106** 013603

[22] Roussev R V, Langrock C, Kurz J R and Fejer M M 2004 Periodically poled lithium niobate waveguide sum-frequency generator for efficient single-photon detection at communication wavelengths *Opt. Lett.* **29** 1518–20

[23] VanDevender A P and Kwiat P G 2004 High efficiency single photon detection via frequency up-conversion *J. Mod. Opt.* **51** 1433–45

[24] Langrock C, Diamanti E, Roussev R V, Yamamoto Y, Fejer M M and Takesue H 2005 Highly efficient single-photon detection at communication wavelengths by use of upconversion in reverse-proton-exchangend periodically poled LiNbO$_3$ waveguides *Opt. Lett.* **30** 1725–7

[25] Albota M A and Robinson B S 2010 Photon-counting 1.55 μm optical communications with pulse-position modulation and a multimode upconversion single-photon receiver *Opt. Lett.* **35** 2627–9

[26] Huang J and Kumar P 1992 Observation of quantum frequency conversion *Phys. Rev. Lett.* **68** 2153–6

[27] Tanzilli S, Tittel W, Halder M, Alibart O, Baldi P, Gisin N and Zbinden H 2005 A photonic quantum information interface *Nature* **437** 116–20

[28] Van Denvender A P and Kwiat P G 2007 Quantum transduction via frequency upconversion (invited) *J. Opt. Soc. Am.* B **24** 295–9

[29] Rakher M T, Ma L, Slattery O, Tang X and Srinivasan K 2010 Quantum transduction of telecommunications-band single photons from a quantum dot by frequency upconversion *Nat. Photonics* **4** 786–91

[30] McGuinness H J, Raymer M G, McKinstrie C J and Radic S 2010 Quantum frequency translation of single-photon states in a photonic crystal fibre *Phys. Rev. Lett.* **105** 093604

[31] Koshino K 2009 Down-conversion of a single photon with unit efficiency. *Phys. Rev.* A **79** 013804

[32] Ding Y and Ou Z Y 2010 Frequency downconversion for a quantum network *Opt. Lett.* **35** 2591–3

[33] Takesue H 2010 Single-photon frequency down-conversion experiment *Phys. Rev.* A **82** 013833

IOP Institute of Physics **ΦDP** DEUTSCHE PHYSIKALISCHE GESELLSCHAFT

[34] Dayan B, Pe'er A, Friesem A A and Silberberg Y 2004 Two photon absorption and coherent control with broadband down-converted light *Phys. Rev. Lett.* **93** 023005

[35] Pe'er A, Dayan B, Friesem A A and Silberberg Y 2005 Temporal shaping of entangled photons *Phys. Rev. Lett.* **94** 073601

[36] Dayan B, Bromberg Y, Afek I and Silberberg Y 2007 Spectral polarization and spectral phase control of time-energy entangled photons *Phys. Rev.* A **75** 043804

[37] Kielpinski D, Corney J F and Wiseman H M 2011 Quantum optical waveform conversion *Phys. Rev. Lett.* **106** 130501

[38] Barnett S M and Radmore P M 1997 *Methods in Theoretical Quantum Optics* (Oxford: Oxford Science)

[39] Loudon R 2000 *The Quantum Theory of Light* 3rd edn (Oxford: Oxford Science)

[40] Blow K J, Loudon R and Phoenix S J D 1990 Continuum fields in quantum optics *Phys. Rev.* A **42** 4102–14

[41] Raymer M G, van Enk S J, McKinstrie C J and McGuinness H J 2010 Interference of two photons of different color *Opt. Commun.* **283** 747–52

[42] Strake E, Bava G P and Montrosset I 1988 Guided modes of Ti:LiNbO$_3$ channel waveguides: a novel quasi-analytical technique in comparison with the scalar finite-element method *J. Lightwave Technol.* **6** 1126–35

[43] Wasilewski W, Lvovsky A I, Banaszek K and Radewicz C 2006 Pulsed squeezed light: simultaneous squeezing of multiple modes *Phys. Rev.* A **73** 063819

[44] Christ A *et al* unpublished work

[45] Branczyk A M, Fedrizzi A, Stace T M, Ralph T C and White A G 2011 Engineered optical nonlinearity for quantum light sources *Opt. Express* **19** 55–65